Dependence of the drag over superhydrophobic and liquid infused surfaces on the asperities of the substrate

Edgardo J. García-Cartagena, Isnardo Arenas, Jaehyeong An, and Stefano Leonardi

Phys. Rev. Fluids **4**, 114604 — Published 11 November 2019

DOI: 10.1103/PhysRevFluids.4.114604

Dependence of the drag over super hydrophobic and liquid infused surfaces on the asperities of the substrate

Edgardo J. García-Cartagena

Dept. Mech. Engineering, The University of Texas at Dallas, USA

Isnardo Arenas

Dep. de ciencias básicas, Unidades Tecnológicas de Santander; Bucaramanga, Colombia

Jaehyeong An and Stefano Leonardi*

Dept. Mechanical Engineering, The University of Texas at Dallas, USA

(Dated: October 11, 2019)

Abstract

Direct numerical simulations (DNS) of two superposed fluids in a turbulent channel flow with a textured surface made of pinnacles of random height have been performed at $Re_\tau \approx 180$ and $Re_\tau \approx 395$. The texture reproduces an etched sand blasted aluminum. The viscosity ratio between the two fluids is either $m = 0.02$, mimicking the viscosity ratio of a super-hydrophobic surface (water over air), or $m = 0.40$ (water over heptane) resembling a liquid infused surface. A parametric study has been carried out varying the position of the interface between the two fluids to assess the contribution to the drag of the portion of the texture emerging above the interface and provide guidelines for design. Simulations with a deformable interface, at Weber numbers $We^+ \approx 10^{-2}$ and 10^{-3} have been performed. Results have been compared to those obtained assuming the ideal case of a flat interface which is slippery in the streamwise and spanwise direction, (corresponding to a Weber number $We = 0$). The time averaged position of the interface has been correlated to the pressure pressure field induced by the random height pinnacles while, the instantaneous deformation is due to the passage of the near wall coherent structures. We attempted to reconcile the effect of SHS and LIS on the coherent structures by calculating how the shear rate parameter depends on the amount of drag reduction.

* stefano.leonardi@utdallas.edu

I. INTRODUCTION

While a number of different mechanisms have been proposed over the years for turbulent drag reduction, super-hydrophobic (SHSs) and liquid infused surfaces (LISs) have recently shown potential to reduce the drag significantly [1–3]. SHS consists of a textured surface (commonly micro-ridges or micro-posts) with a thin film hydrophobic coating that increments the motion of water drops by reducing their contact-angle hysteresis. The physical principle is to reduce skin-friction drag by sustaining a shear-free air-water interface over which water can slip. A valid alternative to the use of SHSs is represented by liquid infused or impregnated surfaces that are conceptually similar, except for the infusion of a second liquid that replaces the air pockets in the surface features. These surfaces take advantage of the greater robustness of the liquid-liquid interface and they are known to be self-healing with exceptional liquid- and ice-repellency and pressure stability [4].

An economical viable technique to produce SHSs and LISs is through spray coating or sandblasting with etching. The resulting textured surfaces have a random distribution of concave valleys and asperities [5–7]. It has been shown that such textures can sustain drag reduction under turbulent flows [8]. However, experiments have also underlined the importance of the surface roughness with respect to the viscous sublayer. The substrate can be thought as a rough wall and the roughness scale plays a crucial role in determining the amount of drag reduction. As the Reynolds number increases there is a loss of drag reduction performance if the surface roughness is not sufficiently small [6].

It has been demonstrated extensively that when the lubricant is lost and the substrate transitions from Cassie state to Wenzel state, the texture behaves as a rough surface, actually increasing the drag on the flow [5]. The drag reduction performance and stability of random-texture in SHSs has been studied numerically by Seo and Mani [9]. The texture was modeled as a boundary condition with alternating regions of no-slip and free-slip, similar to previous numerical studies [1, 10, 11]. Micro-posts (no-slip regions) randomly placed have been compared with aligned patterns. The deformation of the interface was estimated from the solution of the Young-Laplace equation using the average pressure field obtained with flat interface. This approach was already used in Seo *et al.* [11] and a linearized version coupled

to the overlying turbulent flow in Seo *et al.* [12]. Their results showed that for random posts, pressure fluctuations are higher thus the interface is considered less stable than that relative to aligned pattern texture. The effect of the texture and surface tension on SHS and LIS was also studied by García-Cartagena *et al.* [13] for an array of staggered cubes. The dynamics of the interface was found to have a detrimental effect on the drag reduction performance depending on geometrical parameters of the textured surface and on the Weber number. In both Seo and Mani [9] and García-Cartagena *et al.* [13] the cubes and pillars have a uniform height. However, there is interest in non–uniform textures with randomly placed pinnacles because they are more effective maintaining the lubricant layer in the substrate than microridges or microposts as shown by Kim and Rothstein [14].

In the present paper we consider the case of an etched sand blasted aluminum substrate with a non uniform height distribution of the pillars. Alamé and Mahesh [15] have recently performed DNS of a laminar Couette flow and a turbulent flow with a flat interface for the same texture using a volume of fluids approach. Here we expand on their work by considering a deformable interface fully coupled to the Navier-Stokes equations. We carried out DNS at different Weber and Reynolds numbers for two viscosity ratios between the two fluids to mimic both SHS and LIS. We assess the influence of Reynolds and Weber numbers and viscosity ratio on the slip velocity and on the velocity profiles in Sect. III. In Sect. IV we discuss how the random distribution of the pinnacles affects the pressure field and the deformation of the interface and we attempt to correlate it with the distance from the asperities. In addition, we attempt to quantify the detrimental effect the portion of the texture emerging above the interface has on the drag (Sect. V) to provide guidelines in the design of the texture. How SHS and LIS affect the coherent structures and turbulent intensities is presented in Sect. VI and VII.

II. NUMERICAL METHOD AND GEOMETRICAL CONFIGURATION

The non-dimensional Navier-Stokes equations for two fluid flows can be written as

$$\frac{\partial U_i}{\partial t} + \frac{\partial U_i U_j}{\partial x_j} = -\frac{\partial P}{\partial x_i} + \frac{1}{Re}\frac{\partial}{\partial x_j}\left[\tilde{\mu}(\Phi) 2 S_{ij}\right] + \Pi\delta_{i1} + \frac{1}{We}\kappa n_i \delta(\Phi) \tag{1}$$

$$\frac{\partial U_i}{\partial x_i} = 0 \tag{2}$$

where U_i are the velocity components ($U_1 = U$, $U_2 = V$, $U_3 = W$ are the streamwise, wall–normal and spanwise velocity respectively), P the pressure, $Re = \rho U_b H/\mu_2$ the Reynolds number, U_b is the bulk velocity, H is the half height of the channel, S_{ij} is the strain rate tensor, Π the pressure gradient required to maintain a constant flow rate, $We = \rho H U_b^2/\sigma$ the Weber number, σ interface tension, κ the curvature of the interface and n_i the unit normal along the interface. A signed distance function from the interface Φ is used to mark the two fluids. The interface is implicitly defined by the zero level $\Phi = 0$ iso-surface of this function. The level set method [16] is used to track the motion of the interface between the two fluids. This is done by solving the transport equation:

$$\frac{\partial \Phi}{\partial t} + \frac{\partial (U_i \Phi)}{\partial x_i} = 0, \tag{3}$$

written in conservative form. The discontinuity in the viscosity of the two fluids is defined with the parameter $\tilde{\mu}(\Phi) = m + (1 - m)H_\epsilon(\Phi)$ where $m = \mu_1/\mu_2$ is the viscosity ratio (1 and 2 being the fluid in the substrate and in the main stream respectively) and H_ϵ the Heaviside function. The effect of surface tension is added in the equation (1) as body force using the continuous surface force (CSF) method with the use of a mollified delta function $\delta_\epsilon(\Phi) = dH_\epsilon/d\Phi$. The interface is considered with finite thickness ϵ for numerical stability.

The Navier-Stokes equations are solved with a second-order finite difference scheme, third order Runge-Kutta algorithm for the time stepping combined with the fractional–step method [17]. The level set equation is solved using conservative weighted essentially non-oscillatory (WENO) reconstruction [18] along with a re-initialization method [19] to guarantee mass conservation. The PROST method [20] is used to determine accurately the interface curvature (last term in Eq.1). The interface is assumed to be pinned at the substrate. Because at the substrate the velocity is zero, the level set function does not change in time and the interface remains pinned. The flow inside the valleys is driven mostly by the shear transferred from the overlying flow but also by the external forcing Π (Eq.1) which maintains the flow rate constant. See [21] for the momentum balance in the valley. Direct numerical simulations of two superposed fluids in a turbulent channel with a textured surface made of pillars of random height (Fig. 1) have been carried out. The substrate reproduces the etched sand blasted aluminum (SB-AL) of Pillutla *et al.* [22], and it is modelled by means of the immersed boundary method [23]. The mean height of the surface is $h_{mean} = 0.027H$ and its root mean square (rms) is $h_{rms} = 0.0055H$. The viscosity ratio between the two

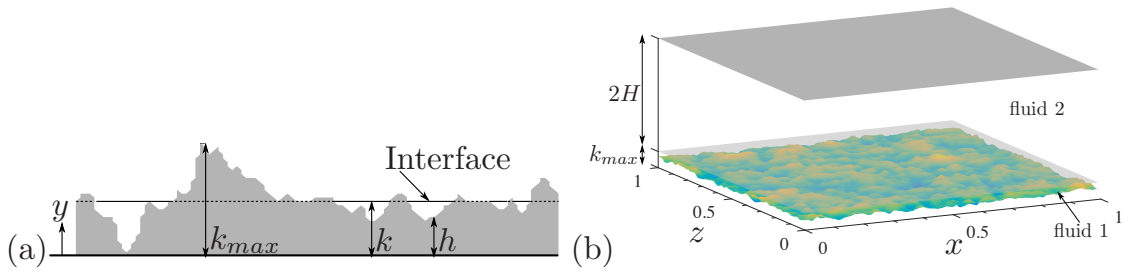

FIG. 1. (a) Sketch of the surface and definitions of k, k_{max}, and h. (b) A portion of the computational domain showing the substrate, the interface between the two fluids and the definition of H.

fluids is either $m = \mu_1/\mu_2 = 0.02$ or 0.4 modeling to some approximation the viscosity ratio of water over air (as in SHS) and heptane (as in LIS), respectively. In the present paper, the density of the two fluids is assumed to be the same ($\rho_1/\rho_2 = 1$) to focus on the effect of the viscosity ratio on the flow.

The computational domain is $7.72H \times 2.05H \times 2.89H$ in the streamwise, wall-normal and spanwise direction respectively. The origin in the vertical direction is set on the bottom valley as shown in Fig.1a. The extra $0.05H$ in the wall-normal direction accounts for the bottom layer with the rough substrate. Periodic conditions are applied in the streamwise and spanwise directions. To conform with this condition, the substrate was tiled with mirroring and appropriate scaling in order to achieve periodicity in these directions, similar to the approach of Thakkar *et al.* [24]. The grid is $1024 \times 384 \times 384$ in the streamwise, wall-normal and spanwise directions, with uniform grid spacing in horizontal directions and stretching in the wall-normal direction.

Two sets of simulations have been performed at $Re = 2,800$ and $6,900$. Three Weber numbers have been considered: $We = 0$ which mimics the ideal case of a flat and slippery interface, and the more realistic cases of $We = 40$ and 400 (corresponding approximately to

TABLE I. Area fraction and volume fraction as a function of interface position

k/k_{max}	0	0.2	0.4	0.6	0.8	1
AF	0	0.0029	0.0913	0.6805	0.9934	1
VF	0	0.0008	0.0170	0.1366	0.3328	0.4660

$We^+ \simeq 10^{-3}$ and 10^{-2} respectively) allowing the interface between the two fluids to deform. For the case of $We = 0$, six cases were considered varying the distance in the vertical direction of the interface from the bottom of the substrate: $k/k_{max} = 0, 0.2, 0.4, 0.6, 0.8, 1$, where the limiting cases of $k/k_{max} = 0$ and 1 represent a rough wall with only one fluid and the ideal

TABLE II. Summary of simulation parameters and representative results

$\langle k \rangle / k_{max}$	m	Re	We	Re_τ	We^+	Ca	DR
0.00	-	2800	-	179.24	-	-	-0.023
0.20	0.02	2800	0	178.43	0	0	-0.013
0.40	0.02	2800	0	179.43	0	0	-0.025
0.60	0.02	2800	0	174.74	0	0	0.028
0.80	0.02	2800	0	112.68	0	0	0.596
1.00	0.02	2800	0	97.25	0	0	0.699
0.20	0.4	2800	0	179.11	0	0	-0.021
0.40	0.4	2800	0	177.27	0	0	0.000
0.60	0.4	2800	0	176.45	0	0	0.009
0.80	0.4	2800	0	162.74	0	0	0.157
1.00	0.4	2800	0	141.61	0	0	0.362
0.00	-	6900	-	402.53	-	-	-0.067
0.20	0.02	6900	0	401.12	0	0	-0.059
0.40	0.02	6900	0	402.46	0	0	-0.067
0.60	0.02	6900	0	383.86	0	0	0.030
0.80	0.02	6900	0	238.37	0	0	0.626
1.00	0.02	6900	0	201.69	0	0	0.732
0.20	0.4	6900	0	401.02	0	0	-0.059
0.40	0.4	6900	0	401.58	0	0	-0.062
0.60	0.4	6900	0	392.36	0	0	-0.014
0.80	0.4	6900	0	329.69	0	0	0.284
1.00	0.4	6900	0	271.23	0	0	0.516
0.75	0.02	2800	40	146.25	7.46×10^{-4}	4.71×10^{-3}	0.319
0.77	0.4	2800	40	168.81	8.61×10^{-4}	1.88×10^{-3}	0.093
0.59	0.02	6900	40	396.60	3.33×10^{-4}	2.25×10^{-4}	-0.039
0.60	0.4	6900	40	398.79	3.35×10^{-4}	1.38×10^{-4}	-0.047
0.64	0.02	2800	400	175.16	8.94×10^{-3}	9.49×10^{-3}	0.023
0.65	0.4	2800	400	177.39	9.05×10^{-3}	7.11×10^{-3}	-0.002
0.59	0.02	6900	400	401.15	3.37×10^{-4}	2.87×10^{-3}	-0.049
0.60	0.4	6900	400	400.75	3.36×10^{-4}	1.43×10^{-3}	-0.057

case of a substrate entirely in the Cassie state with area fraction $AF = 1$ respectively (table I). The area fraction (AF) is defined as the ratio between the liquid lubricant interface area and the total horizontal area of the substrate ($AF = A_{lubricant}/A_{total}$), and listed in table I for all the interface positions. The definition of area fraction is reported as reference in addition to the more meaningful volume fraction because in most numerical studies, the volume below the interface is not considered. Details of the numerical simulations, such as the turbulent Reynolds number $Re_\tau = u_\tau H/\nu$, capillary numbers defined as $We^+ = \mu_2 u_\tau/\sigma$ and $Ca = \mu_2 \overline{U}_{slip}/\sigma$ and the amount of drag reduction $DR = (\tau_0 - \tau_w)/\tau_0$ ($\overline{U}_{slip}$ is the slip velocity, $u_\tau = \sqrt{\tau_w/\rho_2}$ is the friction velocity, τ_w is the total shear stress on the substrate, τ_0 the shear stress of a smooth wall with the same Reynolds number) are summarised in Table II.

III. VELOCITY STATISTICS

Mean velocity profiles in wall units are shown in Fig. 2. The angular brackets indicate averages in time while an overbar denotes averages in time and in the horizontal directions excluding points inside the roughness. A plus indicates normalization by either u_τ or ν/u_τ for velocities and distances respectively. Experimental results obtained over etched sand blasted aluminum [26] SHS and smooth wall data from Moser *et al.* [25] are also included as reference. The origin in the vertical direction for rough wall is usually set between the bottom of the texture and the crests such that the slope of the log-region is $\kappa = 0.41$ [27]. Different choices of the vertical origin provide a slightly different slope of the log-region. For example, Leonardi *et al.* [28] showed that setting the origin at the centroid of the moments (as suggested by Jackson [29]) provides a slope which varies between $\kappa \simeq 0.33$–0.47. Similarly, it is somewhat arbitrary the choice of a vertical origin in SHS-LIS. However, since in the present paper the focus is on the detrimental effect of the asperities on the reduction of drag, and on the comparison between different textures, we set for all cases the origin at the mean height of the substrate, $h_{mean} = 0.54 k_{max}$. Because the size of the substrate here is about 10 and 20 wall units for $Re_\tau \simeq 180$ and 395 respectively, the uncertainty in the position of the origin is between 5 and 10 wall units and does not affect the trends and general conclusions discussed in the following sections.

For the ideal case of slippery interface ($We = 0$), the log-region is shifted upward with

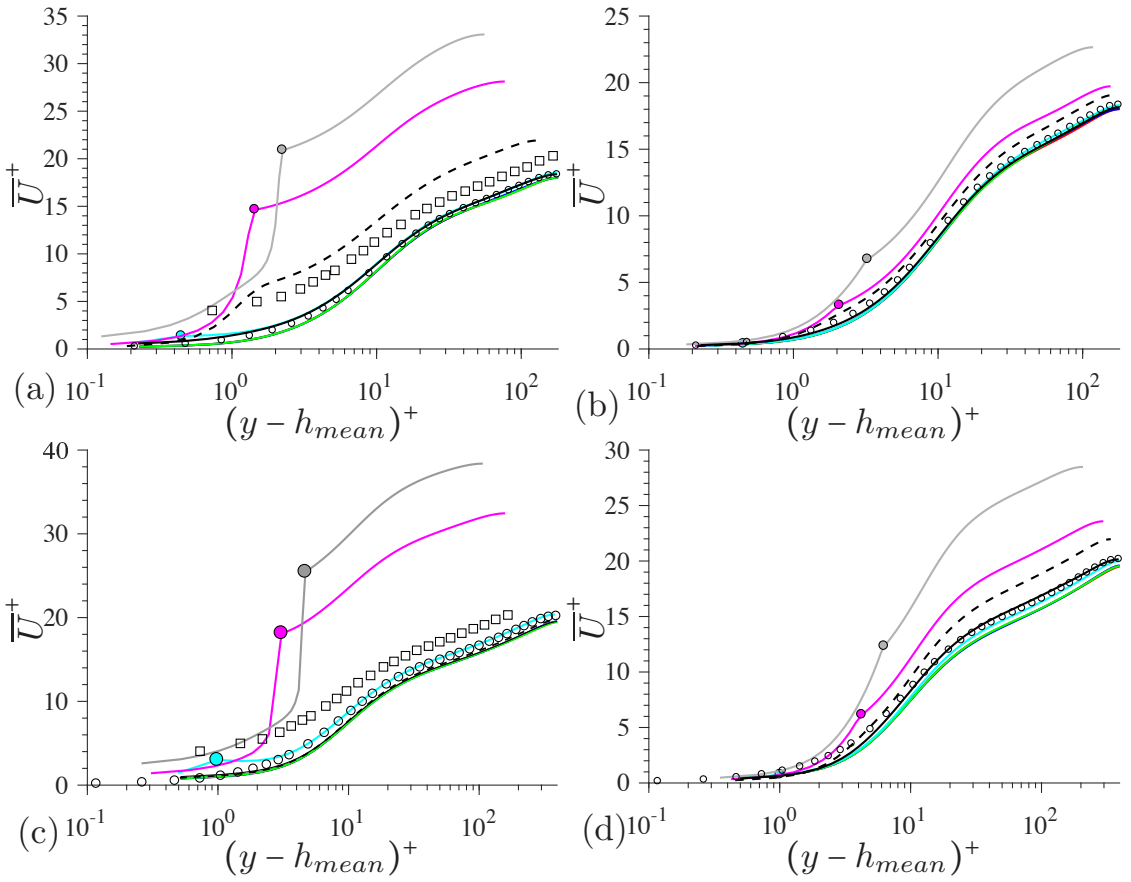

FIG. 2. Mean velocity profiles in wall units for $m = 0.02$ (a,c) and $m = 0.4$ (b,d) at $Re_\tau = 180$ (a,b), and at $Re_\tau \approx 395$ (c,d) (the Re_τ of each case is provided in Table II) for $We = 0$: $k/k_{max} = 0$ (—), $k/k_{max} = 0.2$ (—), $k/k_{max} = 0.4$ (—), $k/k_{max} = 0.6$ (—), $k/k_{max} = 0.8$ (—), $k/k_{max} = 1$ (—); for $We^+ \approx 10^{-3}$: $\overline{k}/k_{max} = 0.755$ (- - -) and for $We^+ \approx 10^{-2}$: $\overline{k}/k_{max} = 0.637$ (—). Velocity profiles of a smooth channel flow with the corresponding Re_τ from Moser *et al.* [25] (○) and over SHS etched sand blasted aluminum (SB-AL) at $Re_\tau \approx 700$ from Ling et al. [26] (□) are included as reference. The interface position is indicated with (●). For the cases $k/k_{max} < 0.6$ the interface is not shown in the figure because is below $(y - h_{mean})^+ = 0.1$.

respect to the smooth wall data when the position of the interface is $k/k_{max} \simeq 0.8 - 1$. This is due to a reduced wall shear stress and to a slip velocity (circle symbols in the figure) at the interface between the two fluids. As expected, idealised SHS present a slip velocity larger than that over a LIS at the same Reynolds number and with the same position of the interface. For the SHS, the slip velocity is in the range $\overline{U}^+_{slip} = 15 - 20$ while for LIS is about $\overline{U}^+_{slip} = 4 - 12$. When the interface is placed at $k/k_{max} \simeq 0.6$ and $We = 0$, the mean velocity

profile agrees well with that of a smooth channel for both viscosity ratios and Reynolds numbers. If the interface is placed further downward, $k/k_{max} < 0.6$, the log-region is slightly shifted downward with respect to the smooth wall, similarly to the flow over rough surfaces in the hydro-dynamically smooth regime. This downward shift is more noticeable for the case of LIS with $Re_\tau \approx 395$. Two cases with deformable interface were also simulated and included in Fig. 2, $We^+ \approx 10^{-3}$ and 10^{-2}. The simulations were initialized with the last velocity field obtained at $We = 0$ and $k/k_{max} = 0.8$. After a transient, the interface oscillates around a new position of equilibrium (shown in Sect. IV) ranging between $0.6 \leq \overline{k}/k_{max} \leq 0.76$ depending on the Reynolds number and viscosity ratio of the two fluids (the overbar indicates the time and space averaged distance between the interface and the bottom wall). The velocity profiles relative to $We^+ \approx 10^{-2}$ overlap closely to that relative to the smooth wall, while the velocity profiles for $We^+ \approx 10^{-3}$ are shifted upward, although much less than those for $We = 0$. Although the asperities are relatively similar to the case with flat interface ($We = 0$) with $\overline{k}/k_{max} = 0.8$, the upward shift is significantly reduced because the friction velocity is larger when the interface can deform. As discussed in [21], this is due to the larger momentum transfer inside the texture induced by wall normal velocity fluctuations at the interface which instead for $We = 0$ are zero. Among the cases with a deformable interface, the configuration with $Re_\tau \approx 180$, $m = 0.02$ and $We^+ = 10^{-3}$, corresponding to $\overline{k}/k_{max} = 0.76$, shows the highest upward displacement with respect to the smooth wall.

For $We = 0$ the upward shift of the log-region increases with the Reynolds number. This is also true for LIS with deformable interface and $We = 10^{-3}$ while the opposite occurs for SHS. For SHS with $We = 10^{-3}$, at $Re = 2,800$ the log–region is shifted upward with respect to that of the smooth wall, whereas at $Re = 6,900$ ($Re_\tau \simeq 395$), the velocity profile overlaps to that relative to the smooth wall.

The substrate in the present simulations mimics that in the experiments performed by Ling *et al.* [26] and Ling *et al.* [7], however, the position of the interface was not measured experimentally and a direct comparison is not possible. In addition, the Reynolds number of the experiment was larger than that in the present simulations. Since results in literature indicate that the amount of drag reduction increases with the Reynolds number and with the gas fraction, we can speculate that the time average position of the interface was somewhere between $\overline{k}/k_{max} = 0.64$ and $\overline{k}/k_{max} = 0.76$.

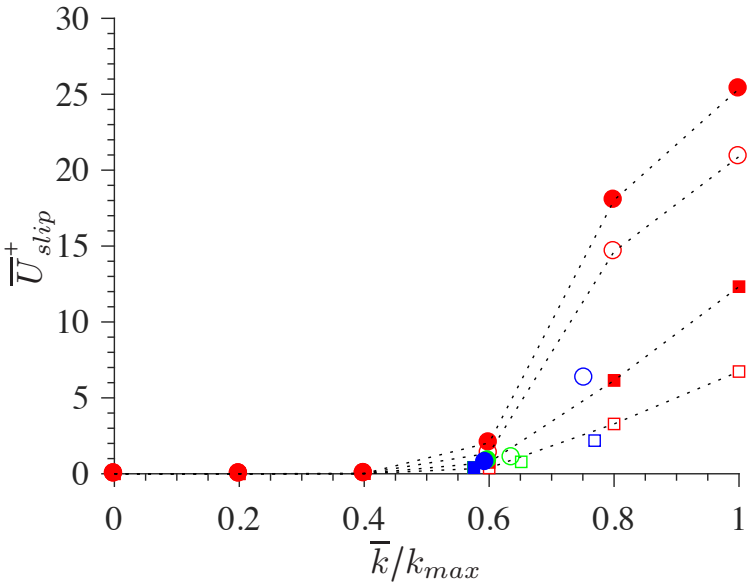

FIG. 3. Slip velocity in wall units as a function of the mean interface position: m = 0.02 (SHS) (○); m = 0.4 (LIS) (□); empty symbols $Re_\tau \approx 180$, filled symbols $Re_\tau \approx 395$; red represents We = 0, green $We^+ \approx 10^{-2}$ and blue $We^+ \approx 10^{-3}$.

Figure 3 shows the slip velocity in wall units for both m = 0.02 and 0.4, mimicking the viscosity ratio of SHS and LIS respectively, for different Reynolds and Weber numbers. In case of $We \neq 0$ it is computed at the location of the time and space averaged interface position $\overline{k}$ (note that for We = 0, $\overline{k} = k$ because the interface does not deform). The slip velocity increases by increasing $\overline{k}/k_{max}$, corresponding to a higher interface position and then to a higher gas fraction and less asperities above the interface itself. The slip velocity is larger for m = 0.02 (SHS) than for m = 0.4 (LIS) as a result of the lower shear at the wall. For a given viscosity ratio, it also increases with the Reynolds number as already noted in literature. When the interface deforms as a consequence of $We \neq 0$, the slip velocity is much lower than the corresponding case at same $\overline{k}/k_{max}$ and Re number. Remarkable is the reduction of slip velocity for $\overline{k}/k_{max} \simeq 0.8$ between the ideal case of We = 0 and the more realistic case with $We^+ \approx 10^{-3}$.

IV. MEAN PRESSURE FIELD AND INTERFACE DEFORMATION

The pressure field on the interface between the two fluids is shown in Fig.4 for We = 0 and We = 40 ($We^+ \simeq 10^{-3}$). The windward face of the asperities presents high pressure

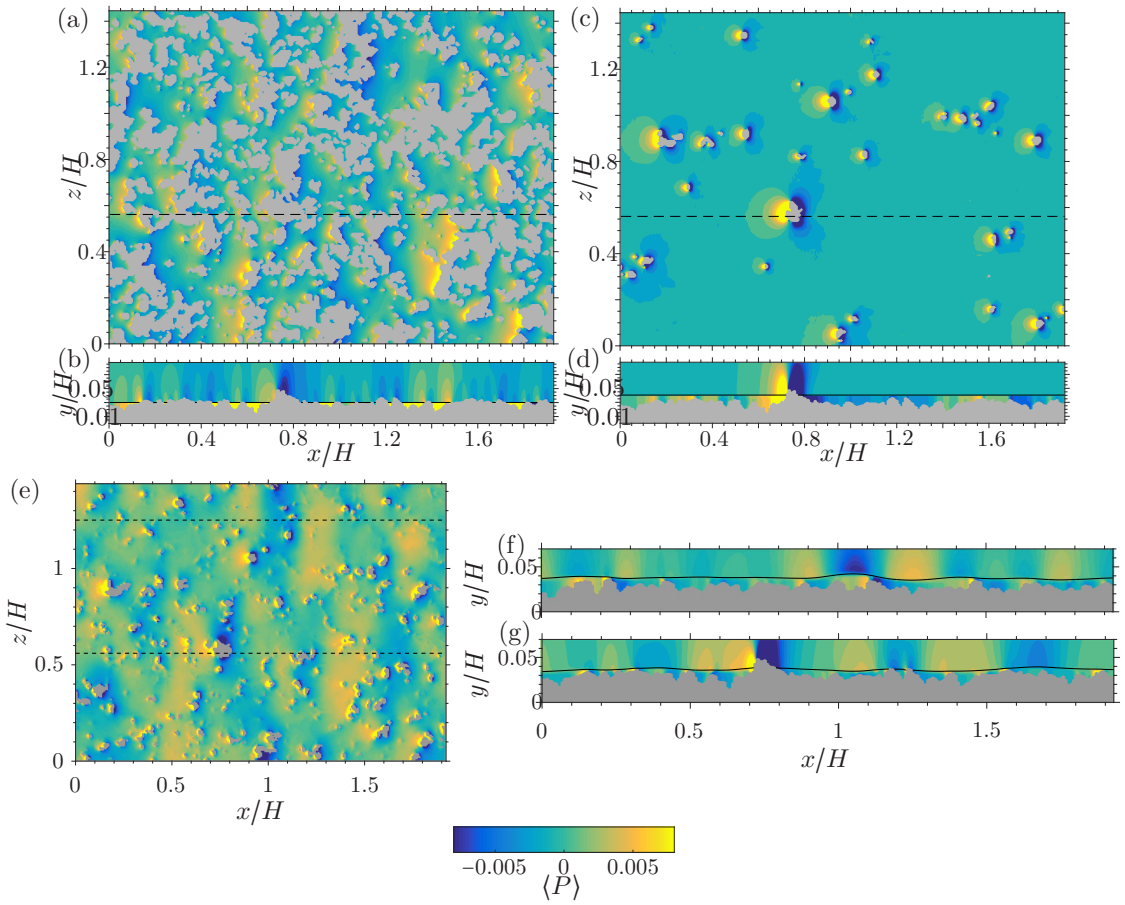

FIG. 4. Color contours of time averaged pressure: (a-d) Re = 2800, m = 0.02 (SHS) and We = 0, (e-g) Re = 2800, We = 40, $\overline{k}/k_{max}$ = 0.75. For We = 0, two interface positions are shown: (a,b) k/k_{max} = 0.6 and (c,d) k/k_{max} = 0.8. Vertical sections are shown at z/H = 0.56 (b,d) for We = 0, and z/H = .56 and 1.25 (f,g) for We = 40.

while low pressure is observed on the leeward side. The closer is the interface to the higher peaks ($k/k_{max} \simeq 0.8$ as in Fig. 4c-d), the larger is the slip velocity and as a consequence the difference between the pressure around the asperities and the surrounding flow. For $k/k_{max} \simeq 0.8$, strong localized pressure gradient occurs near the peaks of the substrate. On the other hand, for $k/k_{max} \simeq 0.6$ a larger portion of the texture emerges out of the interface with an overall larger pressure disturbance to the overlying flow.

A slight deformation of the interface, as that relative to $We^+ = 10^{-3}$ (Fig. 4e,f,g), is such that a small portion of the substrate becomes wet and as a consequence, the pressure inhomogeneity increases and penetrates more into the mean stream.

These localized pressure gradients deform the interface (Fig. 5). The viscosity ratio

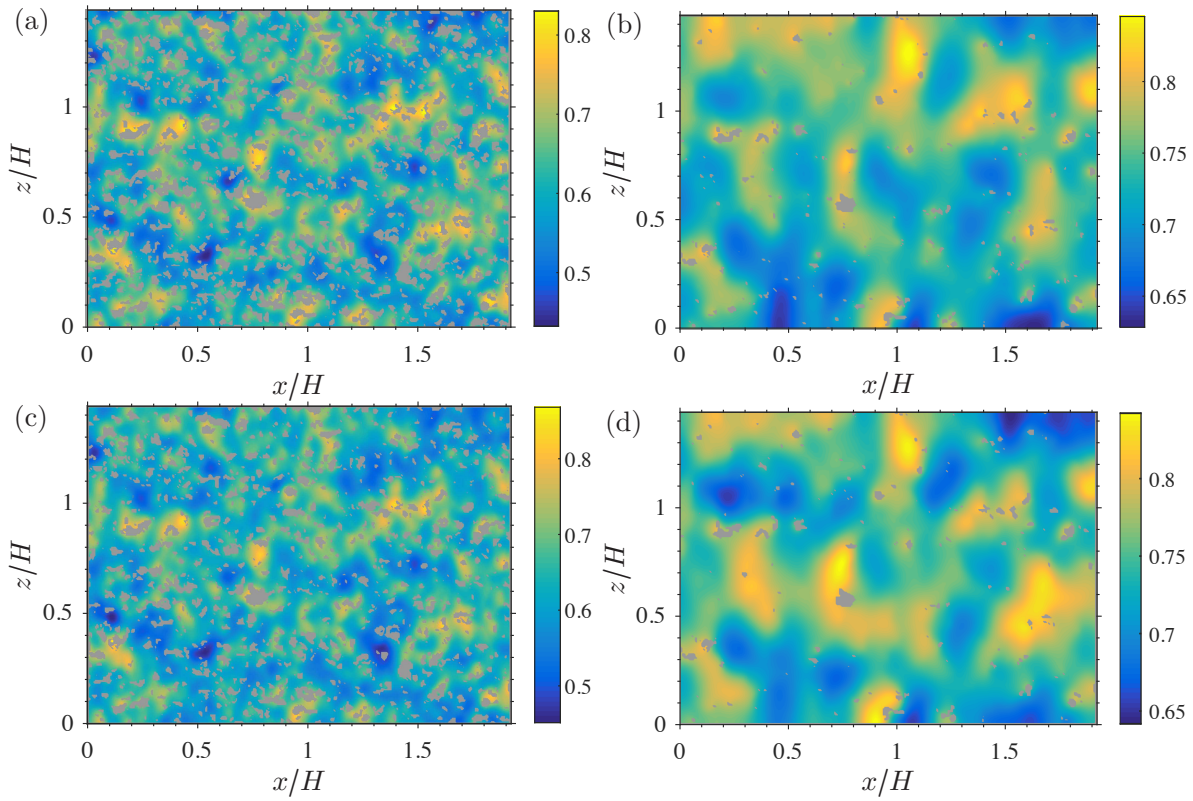

FIG. 5. Color contours of time averaged interface position $\langle k \rangle / k_{max}$ for Re = 2800: a,b) m = 0.02 (SHS), c,d) m = 0.40 (LIS), a,c) We = 400, b,d) We = 40.

does not affect much the time-averaged position of the interface, which for SHS and LIS is qualitatively the same. In our previous studies, [13] with constant height cubes, uniformly distributed in x and z, the deformation of the interface for idealised SHS was significantly larger than that over LIS. However, for the present texture the pressure at the asperities seems to dominate and as a consequence the differences between SHS and LIS are much smaller. It must also be noticed that because the simulations were performed at constant flow rate, the Re_τ for m = 0.02 (SHS) is much smaller than that for m = 0.4 (LIS) as reported in Table 2.

To an increase of the Reynolds number corresponds a downward displacement of the interface between the two fluids. Hence, more asperities emerge above the interface thus reducing the pitch between them and the width of the valleys. As shown in Fig. 4, when the interface is pinned at the higher peaks, (i.e. Fig. 4f $x/H \simeq 1.1$), the pressure is larger below the interface which is therefore lifted upward with a negative concavity. The opposite occurs when asperities emerge out of the interface. The stagnation pressure on the pinnacle

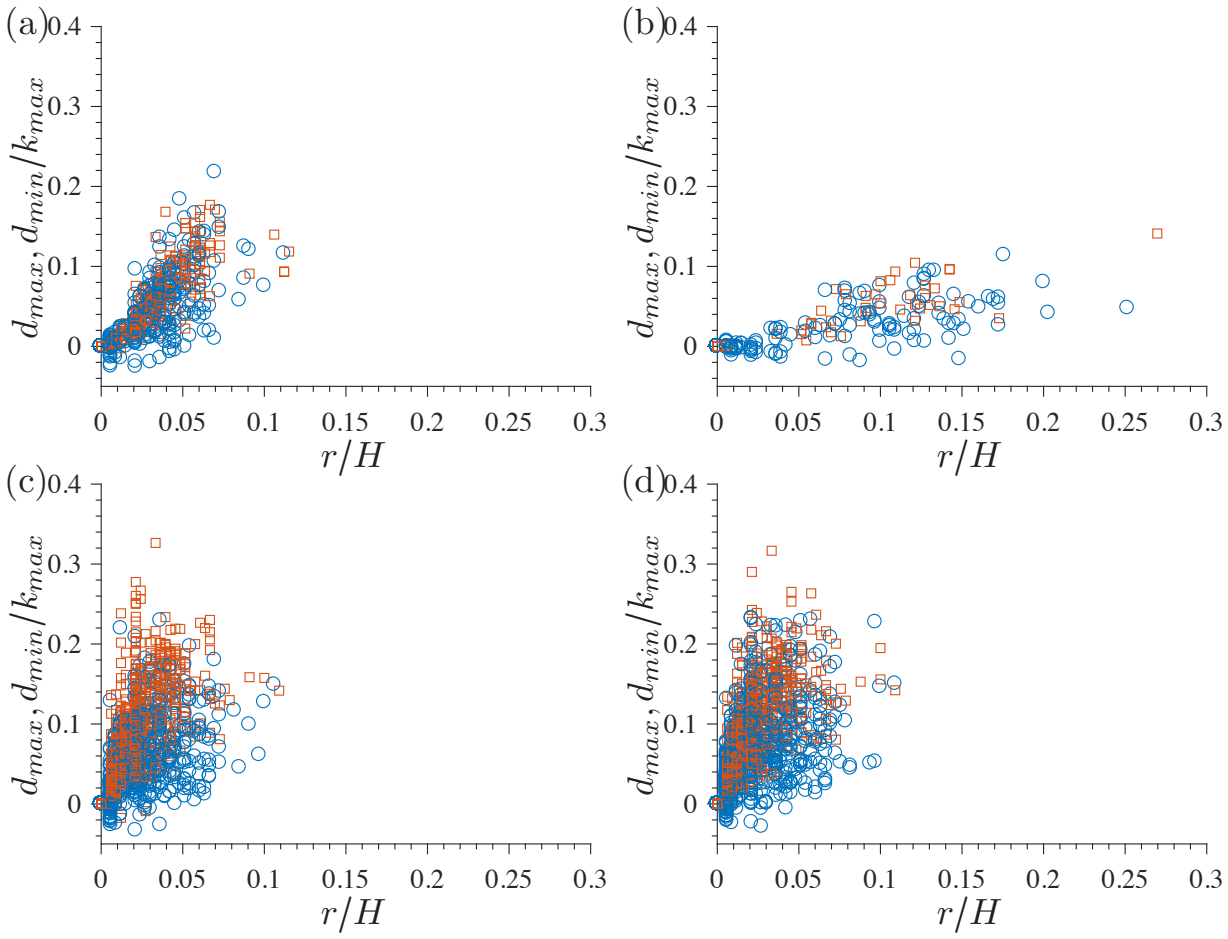

FIG. 6. Maximum and minimum time–averaged displacement with respect to the closest asperity as a function of the equivalent width of the valleys: a,b) Re = 2800, c,d) Re = 6900; a,c) We = 400, b,d) We = 40;○ m = 0.02 (SHS) and □ m = 0.4 (LIS).

induces a downward deformation of the interface (i.e. Fig. 4g $x/H \simeq 0.8$). Therefore, to a good approximation, the interface is displaced downward, (blue contours in Fig. 5) where there are large concave valleys (distance from asperities is large in every direction) and it is lifted upward where the peaks of the substrate are closer. To quantify this, we identified the local maximum and minimum of the displacement $d_{max} = \max[|\langle\Phi(x,\overline{k},z)\rangle|] - d_0$, $d_{min} = \min[|\langle\Phi(x,\overline{k},z)\rangle|] - d_0$, with d_0 being the position of the interface at the closest asperity. The values of d_{max} and d_{min} provide a measure of the waviness of the time-averaged interface. Since the pinnacles have a random distribution, an equivalent width of the valleys was calculated as the distance r between the point where d_{max} or d_{min} are taken and the closest asperity. It must be acknowledged that to the same r may correspond valleys of

different aspect ratios, partially or completely bounded by asperities. However, despite this uncertainty in measuring an equivalent size of the valleys, there is a good correlation between the deformation and r as shown in Fig. 6. The deformation of the interface increases almost linearly with the "equivalent" width of the valley r. The slope increases by increasing either the Weber or Reynolds numbers. In fact, an increase of the Weber number implies a reduced surface tension which opposes the interface deformation. On the other hand, pressure fluctuations increase with the Reynolds number inducing an increased displacement. At $Re_\tau \simeq 180$ and $We = 40$ ($We^+ \simeq 10^{-3}$) the maximum displacement in correspondence of the largest valleys is about $0.1k_{max}$. The equivalent radius of the largest valleys is of the order of $0.25H$, about 5 times the thickness of the texture. The size of the valleys and the maximum displacement in wall units, at this Reynolds number are about $r^+ \simeq 40$ and $d^+_{max} \simeq 1.5$. However, at larger Reynolds numbers or Weber numbers, the waviness is quite large, especially compared to uniform textures studied in the past. The displacement of the interface with respect to the mean is of the order of $20-30\%$ of the maximum height of the substrate. For example for $Re = 6,900$ and $We = 400$, the maximum displacement is about 10 wall units in correspondence of valleys of $r^+ \simeq 25-30$. As shown in Fig. 6 and already inferred qualitatively from Fig.5, the equivalent width of the valleys reduces by increasing the Reynolds number and Weber numbers. In addition, negative displacements (meaning an upward deformation of the interface) are limited to small values of r, hence to small valleys. From the color contours of pressure, in fact, it was observed that near the asperities the interface is tilted upward because of a larger pressure in the valleys.

V. DRAG REDUCTION

The slip length b, the distance where the velocity would be zero by linearly extrapolating the velocity gradient at the interface, $b = \overline{U}_{slip}/(\partial\overline{U}/\partial y)|_{y=\overline{k}}$, has been used to characterize the drag reduction [30, 31]. Rastegari and Akhavan [10] developed a correlation between DR and slip length

$$\boldsymbol{DR = b^{+0}/[b^{+0} + (Re/Re_{\tau_0})] + O(\epsilon)} \; . \tag{4}$$

A subscript or superscript with a "0" denotes normalization using the friction velocity of the smooth wall at the same Reynolds number. Numerical results agree well with the analytical

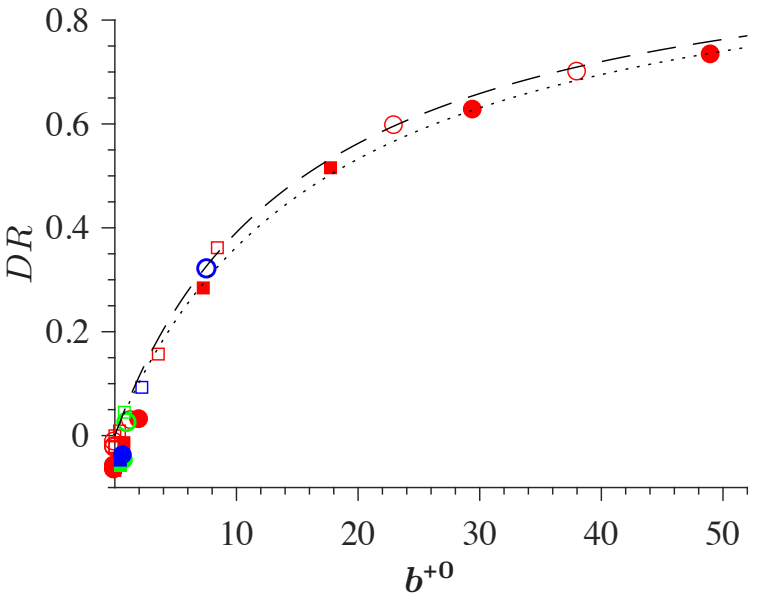

FIG. 7. Drag reduction as a function of the slip length b^{+0} in wall units: m = 0.02 (SHS) (○); m = 0.4 (LIS) (□); empty symbols $Re_\tau \approx 180$, filled symbols $Re_\tau \approx 395$; (---) analytic result with Re_τ = 180 and (·····) with Re_τ = 395 from Rastegari and Akhavan [10]; red color represent We = 0, green $We^+ \approx 10^{-2}$ and blue $We^+ \approx 10^{-3}$.

expression $DR = b^{+0}/[b^{+0} + (Re/Re_{\tau_0})]$ (equation 4 with $\epsilon = 0$) as shown in Fig.7 for different Reynolds numbers, viscosity ratios (mimicking that over SHS and LIS) and Weber number. The agreement is even better than that in our previous study with a uniform array of cubes [13], implying that ϵ, which accounts for the secondary motion, for the present case is much smaller. For $We \simeq 10^{-2}$ and small values of slip length, the amount of drag reduction is over-predicted by the model; in fact, in these cases the drag is slightly larger than that over a flat wall ($DR < 0$). On the other hand, for $We = 10^{-3}$ and $\overline{k}/k_{max} = 0.75$ the slip length is $b^{+0} \simeq 10$ and numerical results agree very well with the model. This is mainly because the total drag is dominated by the viscous part and, in addition, asperities increase the drag, but also reduce the slip length by the induced pressure gradient near it, consistently with the model of Rastegari and Akhavan [10].

Drag reduction as a function of the position of the interface is shown in Fig. 8(a) for both viscosity ratios m = 0.02 (SHS) and m = 0.4 (LIS), $Re_\tau \approx 180$ and 395 at different Weber numbers. The amount of drag reduction increases by increasing the Reynolds number and by reducing the viscosity ratio of the two fluids only when We = 0 (Fig. 8a). The drag

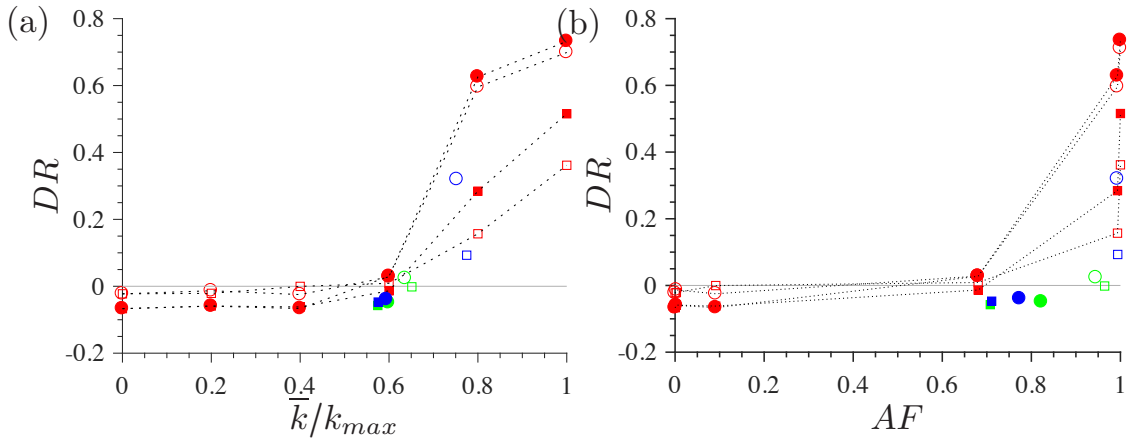

FIG. 8. Drag reduction as a function of the mean interface position, $\overline{k}$, (a) and as a function of the area fraction (b): $m = 0.02$ (SHS) (○); $m = 0.4$ (LIS) (□); empty symbols $Re_\tau \approx 180$, filled symbols $Re_\tau \approx 395$; red $We = 0$, green $We^+ \approx 10^{-2}$ and blue $We^+ \approx 10^{-3}$.

reduction is largest when the interface is on the highest point of the surface $k/k_{max} = 1$ for both surfaces and Reynolds numbers. This corresponds to the ideal case of area fraction $AF = 1$, as shown in Fig.8(b) (where the area fraction is the ratio between the fluid and total surface of the interface). The area fraction for $k/k_{max} = 0.8$ is $AF = 0.99$ (see table I). To such a minor change in area fraction corresponds a drop in the amount of drag reduction of about 10% and 20% for SHS and LIS respectively. This is unexpected from classical studies of SHS-LIS and cannot depend on the small shrinkage of the region where the shear is reduced but rather on resistance caused by the asperities emerging above the interface. In fact, when the position of the interface is below the crests, the amount of drag reduction decreases because part of the substrate becomes wet (as in the sketch in Fig. 1). This could not be assessed in most of previous numerical studies where the texture is not resolved or the crests are at the same height [10, 11, 21, 32]. For $k/k_{max} > 0.8$ the amount of drag reduction is substantial, about 70% for SHS and 45% for LIS for the ideal case of slippery and flat interface ($We = 0$).

The cases with deformable interface ($We^+ \approx 10^{-3}$) present an amount of drag reduction smaller than that obtained with a flat interface ($We = 0$) despite approximately the same area fraction and position of the interface ($\overline{k}/k_{max} \simeq 0.75$). For $k/k_{max} \leq 0.6$, the drag is very close to the value of the smooth wall both in the ideal case of slippery flat interface ($We = 0$) and the more realistic case of deformable interface ($We \neq 0$). The corresponding area

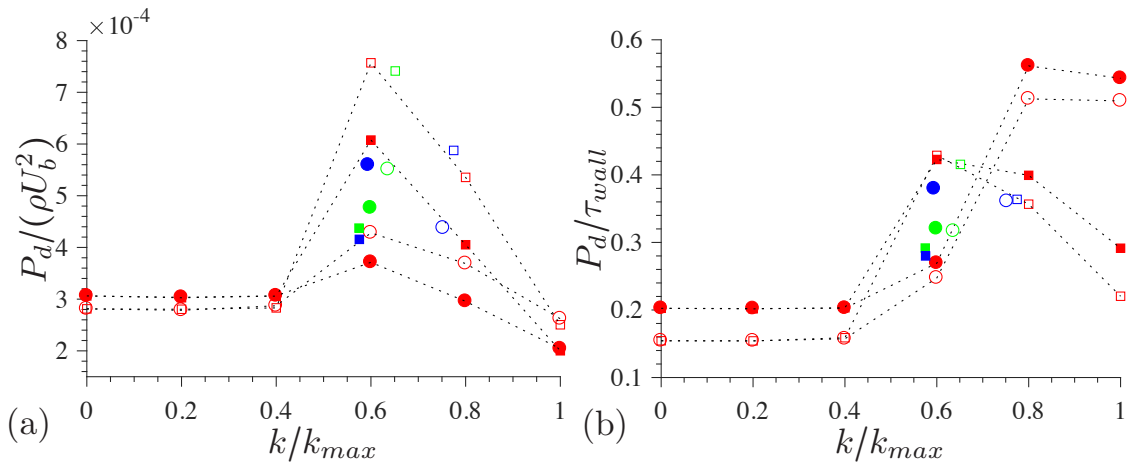

FIG. 9. Form drag (a) and its contribution with respect to the total shear at the wall (b) as function of the position of the interface: $m = 0.02$ (SHS) (○); $m = 0.4$ (LIS) (□); empty symbols $Re_\tau \approx 180$, filled symbols $Re_\tau \approx 395$; red $We = 0$, green $We^+ \approx 10^{-2}$ and blue $We^+ \approx 10^{-3}$.

fraction is about $AF \simeq 0.7$ and, from previous studies in literature [1, 33], one would expect a substantial amount of drag reduction. This is not the case here because the form drag due to the asperities above the interface overcomes the reduction of the viscous shear. The form drag is the sum of two contributions, the pressure drag of the asperities above the interface and that of the valleys below the interface. By integrating the momentum equations, it can be shown that the form drag in the valleys below the interface is proportional to the total shear stress at the interface (the frictional drag on the bottom wall being negligible) [21]. When the interface is pinned at the highest peaks of the substrate ($k = k_{max}$), the form drag is entirely due to the valleys below it. Because for this configuration ($AF = 1$) the DR is maximum, the shear at the interface is small. Therefore the momentum transferred inside the texture and the form drag is also very low as shown in Fig. 9a for both SHS and LIS. If the interface is below the highest peak, such as for $k/k_{max} = 0.6$ and 0.8, asperities emerge above the interface and contribute to the form drag. To some approximation, the form drag scales with the slip velocity and with the height of the asperities above the interface. When the interface is below the highest peaks, there are two opposite effects, a decrease of slip length which tends to reduce the form drag, and an increased wet area of the texture which tends to increase it. When the interface is very close to the bottom wall, the slip velocity is very small and its effect on the pressure drag prevails over the increase in wet area. Therefore, the form drag is maximum when the interface is in an intermediate position

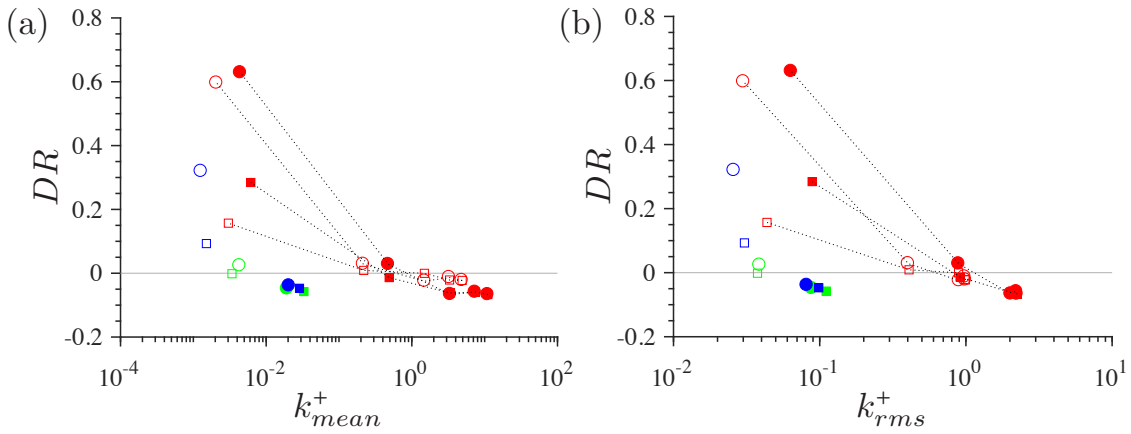

FIG. 10. Drag reduction as a function of the mean surface above the interface normalized in wall units (a) and of its rms (b) for We = 0: m = 0.02 (SHS) (○); m = 0.4 (LIS) (□); empty symbols $Re_\tau \approx 180$, filled symbols $Re_\tau \approx 395$.

between the top of the asperities and the bottom wall. For the cases here considered, for both viscosity ratios a peak of form drag occurs at about k/k_{max} = 0.6. The maximum pressure drag of LIS is larger than that relative to SHS because the shear at the interface and then the momentum transferred inside the valleys is larger than that for SHS. On the other hand, for $k/k_{max} \geq 0.8$, the relative contribution of the form drag to the total drag is much larger for SHS than for LIS. For example, for $k = k_{max}$, the form drag is approximately the same for m = 0.02 and m = 0.4, but for SHS it is the dominant contribution to the total drag (Fig. 9b), about 60% of the total drag being due to the form drag and 40% to the frictional drag. The drag of LIS is, instead, dominated by the viscous drag. The general effect of increasing the Reynolds number is that the form drag decreases, but its contribution to the total drag increases.

Results in Fig.8 and 9 have shown the significance of the asperities and in general of the geometrical features of the substrate. A length scale accounting for this roughness cannot be only function of the geometry of the substrate but also of the position of the interface. While for a single phase flow over rough walls only the shape of the texture matters, in SHS-LIS it is the combination between the texture and the position of the interface to determine the drag. The root mean square of the textured surfaces is h^+_{rms} = 0.99 for Re_τ = 180 and h^+_{rms} = 2.18 for Re_τ = 395. However, the flow behaviour changes considerably with the position of the interface, The amount of drag reduction ranges from 70% to −5% for the

same texture varying the position of the interface despite the same value of h_{rms}. Therefore, h_{rms} is not a proper length scale to characterize the surface. It is the portion of the texture emerging out of the interface the dominant geometrical feature affecting the flow. This can be quantified for example by k_{mean}, the amount of asperities above the interface:

$$k_{mean} = \frac{1}{N} \sum (h(x,z) - k) \mid h(x,z) \geq k \tag{5}$$

and its root mean square:

$$\boldsymbol{k_{rms} = \sqrt{\frac{1}{N} \sum (h(x,z) - k - k_{mean})^2 \mid h(x,z) \geq k}} \, . \tag{6}$$

The value of k_{mean} accounts for the portion of the substrate emerging above the interface while k_{rms} gives a measurement of its variability and therefore of the asperities. Both values are function of the interface position k. Figure 10a shows the amount of drag reduction as a function of k^+_{mean}. The smaller k^+_{mean}, the less asperities emerge out of the interface, the more the drag is reduced. It is found that $k^+_{mean} \leq 1$ is necessary in order to have drag reduction, regardless of the viscosity ratio or Reynolds number. The value of k_{rms} in wall-units for the present simulations ranges from $k^+_{rms} = 0.05 - 2.2$ as the position of the interface or the Reynolds number are varied. The amount of drag reduction decreases by increasing k^+_{rms} (Fig. 10b). For $k^+_{rms} \simeq 0.5 - 1$, the penalty due to the asperities out of the interface balances the reduced shear on the valleys and the overall drag is about the same of the smooth wall. The SHS is more sensitive to the value of k^+_{rms}. In fact, the amount of DR relative to SHS drops quickly at around $k^+_{rms} \simeq 0.5$ (Fig. 10b). This is because the slip velocity is larger than that relative to LIS and therefore the form drag has a larger contribution to the total drag (see Fig.9b). The dependence of the drag on k^+_{rms} and on k^+_{mean} implies that the commonly accepted concept according to which the amount of drag reduction increases with the Reynolds number is true only if the asperities above the interface are negligible. Either way, for a given geometry an increase of Reynolds number may lead to an increase of k^+_{rms} and k^+_{mean} and a corresponding increase of pressure drag which could overcome the reduced shear at the interface. The values of k^+_{rms} and k^+_{mean} provide a quantitative measure which could be used for the design of SHS and LIS for practical applications, once the position of the interface can be estimated to some approximation. The limits $k^+_{rms} < 0.5$ and $k^+_{mean} < 1$ are necessary conditions. In fact even in the ideal case of a slippery flat interface, if these criteria are not met, the drag reduction performances are lost. However,

they are not sufficient conditions to achieve drag reduction. For example, the deformation of the interface may increase the drag even further, and even at $k^+_{rms} < 0.5$ the drag may be larger than that of a smooth wall. The values of $k^+_{rms} \simeq 0.5$ and $k^+_{mean} \simeq 1$ are thresholds above which the drag is unlikely to be reduced. Although further validation is required to generalize these values to any texture, they provide a measure of the accuracy needed in designing a texture and of the sensitivity of the drag to a vertical misalignment of the crests of the texture.

VI. TURBULENT INTENSITIES

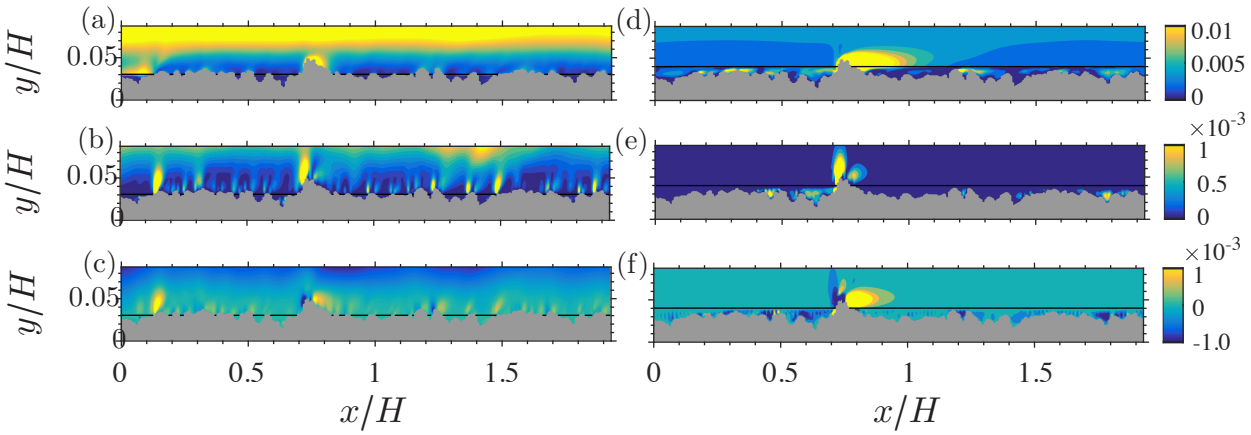

FIG. 11. Color contours of the variance of streamwise velocity fluctuations $\langle uu \rangle$ (a,d), wall-normal velocity fluctuations $\langle vv \rangle$ (b,e) and covariance of streamwise and wall-normal velocity fluctuations $\langle uv \rangle$ (c,f) in a vertical section at $z/H = 0.56$: (a,b,c) correspond to the interface position $k/k_{max} = 0.6$ and (d,e,f) to $k/k_{max} = 0.8$, in both cases $Re_\tau \approx 180$ and $m = 0.02$.

Turbulent intensities and Reynolds shear stress are shown in Fig. 11 near the texture for two positions of the interface ($k/k_{max} = 0.6$ and 0.8), a viscosity ratio $m = 0.02$ (SHS) and a flat interface ($We = 0$). Both $\langle uu \rangle$, $\langle vv \rangle$ and $\langle uv \rangle$ are large in correspondence of the asperities emerging above the interface ($u(x,y,z,t) = U(x,y,z,t) - \langle U(x,y,z) \rangle$, $V(x,y,z,t) = v(x,y,z,t) - \langle V(x,y,z) \rangle$, $w(x,y,z,t) = W(x,y,z,t) - \langle W(x,y,z) \rangle$ and $\langle u_i u_j(x,y,z) \rangle = \frac{1}{N_t} \sum_{n=1}^{N_t} (U_i(x,y,z,t_n) - \langle U_i(x,y,z) \rangle)(U_j(x,y,z,t_n) - \langle U_j(x,y,z) \rangle$, $i = 1,2,3$ corresponds to U, V, W respectively). When the interface is closer to the highest pinnacles ($k/k_{max} = 0.8$ Fig. 11 d,e,f), the turbulent intensities and Reynolds shear stress are rather uniform except

near the pinnacles where a significant increase of the fluctuations is observed ($x/H \simeq 0.75$). In fact, when the interface is closer to the highest asperities, the drag is reduced and the slip velocity is larger. Therefore in most of the texture the fluctuations of velocity decrease. However, due to the high slip velocity, in proximity of the pinnacles above the interface, velocity and pressure gradients are large inducing locally a high turbulence level. The variability of turbulent intensities within the texture is confined to a thin layer above the interface. At about $y/H = 0.05$, one texture height above the interface, turbulent intensities and Reynolds stress do not depend on x/H and the modulation due to the substrate is lost. Therefore, above this height, turbulent intensities and Reynolds stresses are only function of the distance from the wall:

$$\overline{u_i u_j}(y_m) = \frac{1}{N_x N_z N_t} \sum_{l=1}^{N_x} \sum_{k=1}^{N_z} \sum_{n=1}^{N_t} (U_i(x_l, y_m, z_k, t_n) - \overline{U_i}(y_m))(U_j(x_l, y_m, z_k, t_n) - \overline{U_j}(y_m)) \,. \quad (7)$$

The overall effect of LIS-SHS on the turbulent intensities and Reynolds stress is shown in Fig. 12. Regardless of the Weber number, when the interface lies below 60% of the highest peaks ($k/k_{max} < 0.6$), $\overline{uu}^+$, $\overline{vv}^+$ and $\overline{uv}^+$ overlap closely with those relative to the flat wall (figure 12), similarly to what has been observed for the velocity profiles in wall units (figure 2). When the interface is closer to the crests, $k/k_{max} = 0.8$ and 1, $\overline{uu}^+$ presents two peaks, one at the interface and one above it. The fluctuations near the wall are significantly larger than those relative to a flat wall, perhaps surprisingly since these cases present a reduction of the drag. However, the increased velocity fluctuations and the peak at the interface are due to the dispersive stresses induced by the spatial variability of the time averaged flow within the textured surface. The second peak, in the inner part of the channel is due to the near wall coherent structures and it is very similar to that relative to a smooth wall. For $We^+ \approx 10^{-3}$ the slip velocity is much smaller (Fig. 3) and the position of the interface oscillates. As a consequence the spatial inhomogeneities of the flow are weaker, the dispersive stresses are reduced and smoothed out compared to those relative to $We = 0$ with the same gas fraction $k/k_{max} \simeq 0.8$. Near the wall, an increased magnitude of streamwise velocity fluctuations was also measured experimentally by Ling *et al.* [26]. The position of the peak of $\overline{uu}$ measured experimentally is closer to the wall by approximately five wall units than that obtained numerically. This may be due to the difference in Reynolds number.

All the profiles with $k/k_{max} < 0.6$, regardless of the Weber number or interface position, overlap for $(y - h_{mean})^+ > 10$. On the other hand, for larger gas fraction, ($k/k_{max} > 0.8$),

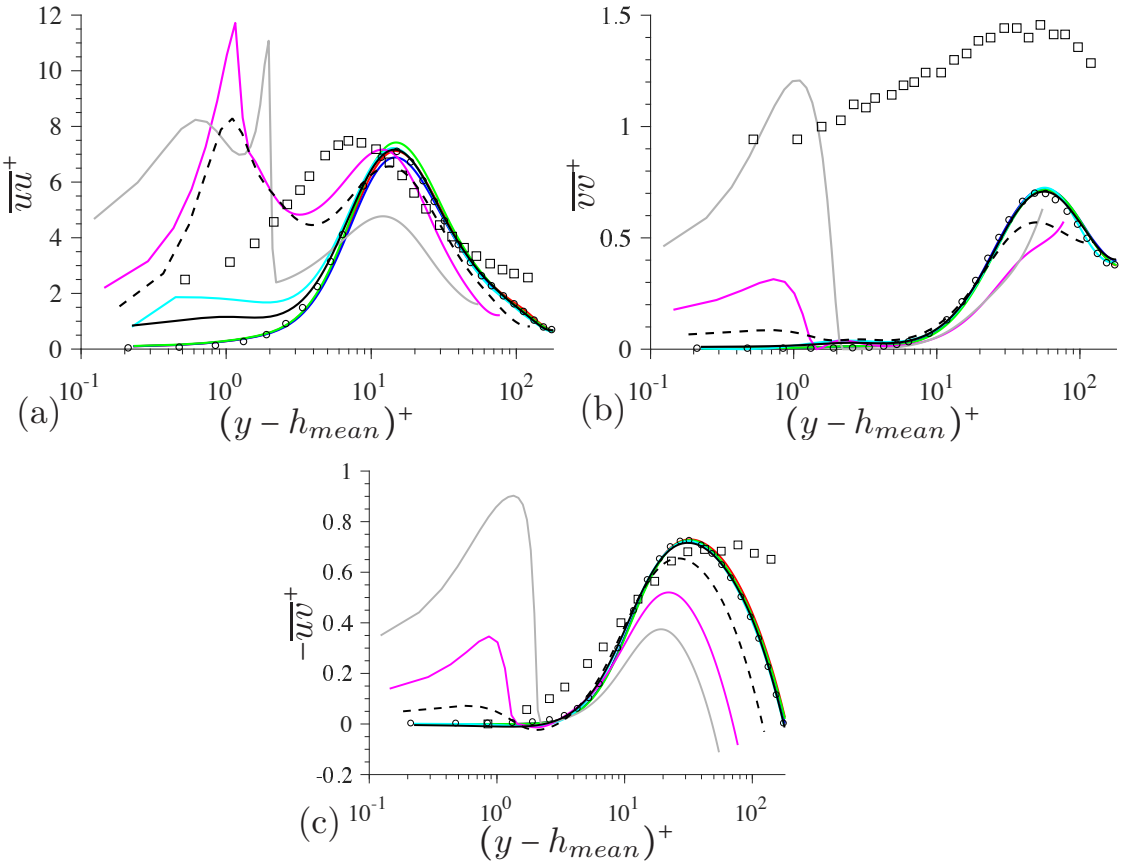

FIG. 12. Variance of streamwise velocity fluctuations (a), Variance of wall-normal velocity fluctuations (b) and Reynolds shear stress (c) for SHS with $Re_\tau \approx 180$, (symbols and lines as in figure 2).

above the wall (for $(y - h_{mean})^+ > 10$), for both $We^+ = 0$ and 10^{-3}, the turbulent intensities are significantly reduced. Interestingly, for $k/k_{max} = 0.8$ and 1, the wall normal velocity fluctuations decrease more than streamwise velocity fluctuation thus increasing the anisotropy. The experimental measurements by Ling *et al.* [26] present larger wall-normal velocity fluctuations than that over smooth wall. In a similar experimental setup (Ling *et al.* [7]), this increased wall-normal velocity fluctuations near the wall was attributed to the transition from smooth to rough wall. The Reynolds shear stress $-\overline{uv}$ obtained numerically with $We^+ = 10^{-3}$ is consistent with experimental data for $10 < (y - h_{mean})^+ \leq 30$. Above the wall, the velocity statistics for LIS are qualitatively similar to SHS, therefore not shown in Fig. 12. However, the dispersive stresses at the walls of LIS are negligible compared to SHS, due to the reduced slip velocity as seen in Fig. 3(b).

VII. TURBULENT COHERENT STRUCTURES

To assess the effect of SHS and LIS on turbulence structures, instantaneous streamwise velocity fluctuations are plotted on a horizontal plane about 10 wall units above the interface at $Re = 2,800$ corresponding to $Re_\tau = 180$ (Fig. 13). Flow structures are highly elongated in the streamwise direction in all cases. However, for $k/k_{max} = 0.6$, the streaks appear shorter and the fluctuations of velocity more intense with respect to those for $k/k_{max} = 0.8$ consistently with the higher shear. For larger Weber numbers, the interface deforms and the amount of drag reduction decreases. For a given Reynolds number, the length and width of the streaks reduce compared to the equivalent case at $We = 0$ and approximately the same $\overline{k}$. In general, reducing the shear results in streaks more elongated and wider in spanwise direction. Because the shear is gradually closer to that of a smooth wall for $We \simeq 10^{-3}$ and 10^{-2}, the streaks resemble more closely those over a smooth wall. Figure 13 also shows the deformation of the interface. There is a good correlation between the deformation of the interface and the streamwise velocity fluctuations. To some approximation, to an upward deformation of the interface (negative level set fluctuation) corresponds a low speed streak. This can be explained with the sketch in Fig. 13i. Counter rotating vortices generating the streaks pull up the interface in proximity of the low speed streaks and push it down in correspondence of the high speed streaks.

TABLE III. Correlation coefficient between level set function fluctuations and streamwise velocity fluctuations at the mean interface position ($\overline{k}$).

Re	We	m	$r_{u\phi}$
2800	40	0.02	0.6024
2800	40	0.4	0.5056
2800	400	0.02	0.6354
2800	400	0.4	0.5763
6900	40	0.02	0.6483
6900	40	0.4	0.6075
6900	400	0.02	0.6804
6900	400	0.4	0.6717

To quantify this correspondence between the streamwise velocity fluctuations, $u(x, y, z, t) = U(x, y, z, t) - \langle U(x, y, z) \rangle$ (streaks), and the displacement of the interface fluctuations,

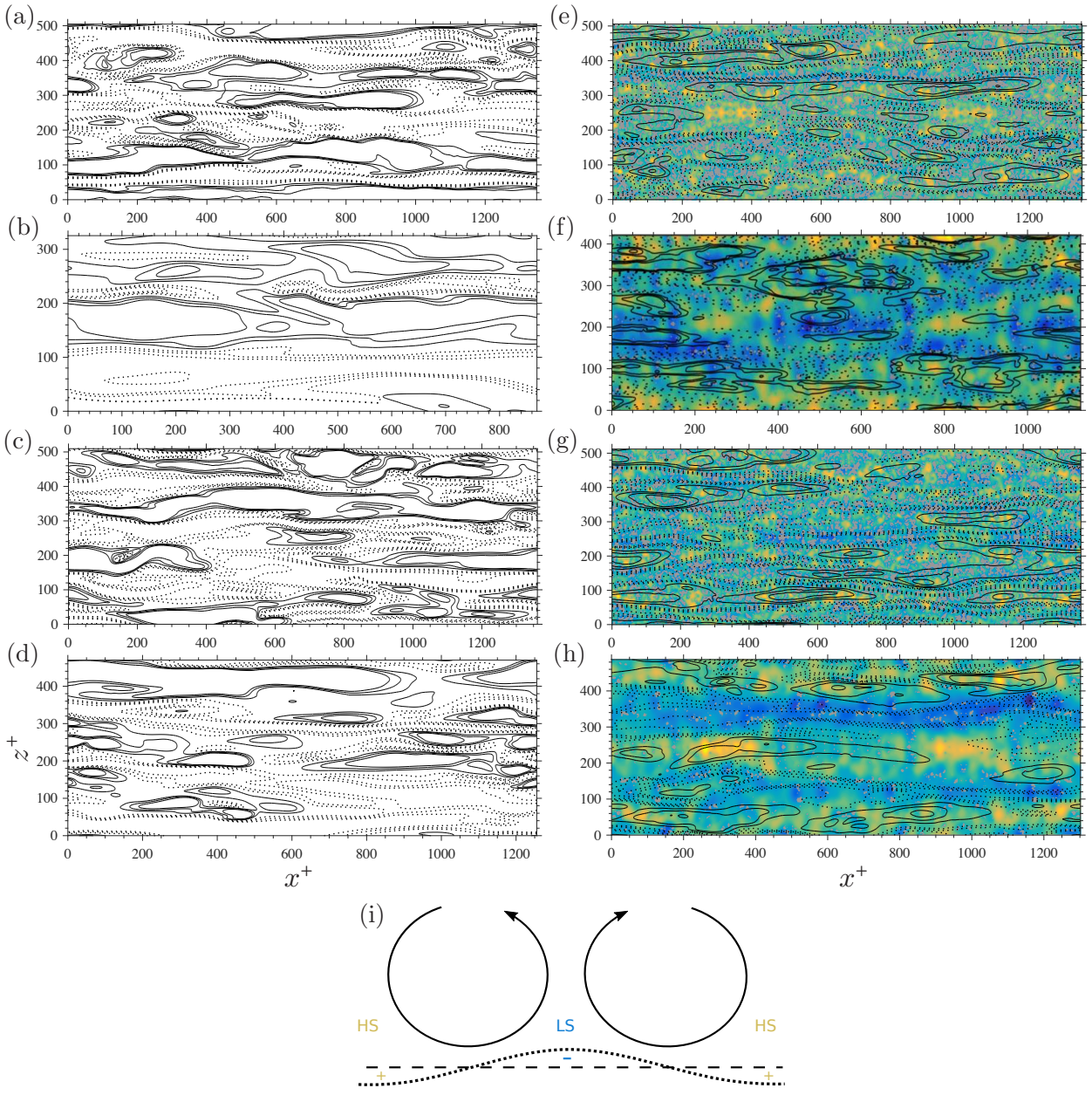

FIG. 13. Iso-contours of streamwise velocity fluctuations at $Re = 2800$ and $We = 0$: (a,c) $k = 0.6$, (b,d) $k = 0.8$. For $We = 10^{-2}$ (e,g) and $We^+ \simeq 10^{-3}$ (f,h), the iso-contours of streamwise velocity fluctuations are superposed to the displacement of the interface with respect to its time-averaged position (e,g) $\overline{k} = 0.6154$, (f,h) $\overline{k} = 0.76$. Two viscosity ratios are shown (a,b,e,f) $m = 0.02$, (c,d,g,h) $m = 0.4$ which mimic idealised SHS and LIS respectively. A sketch of streamwise vortices, low and high speed streaks and deformed interface (dotted line) with respect to the mean interface position $\overline{k}$ is included as reference.

$\phi(x, y, z, t) = \Phi(x, y, z, t) - \langle \Phi(x, y, z) \rangle$, the correlation $r_{\phi u}$ has been computed at the mean

position of the interface $y = \overline{k}$:

$$r_{u\phi} = \frac{\sum_{l=1}^{N_x}\sum_{k=1}^{N_z}\sum_{n=1}^{N_t} u(x_l,\overline{k},z_k,t_n)\phi(x_l,\overline{k},z_k,t_n))}{\tilde{u}\tilde{\phi}} \tag{8}$$

where $\tilde{u}$ and $\tilde{\phi}$ indicate the velocity and interface displacement rms. The values of $r_{u\phi}$ are quite large as reported in Table 3 and confirm the qualitative observation of Fig. 13. The smaller is the Weber number the smaller is the correlation coefficient $r_{u\phi}$. In fact, a smaller Weber number corresponds to a larger surface tension and therefore an interface that tends to resist more to deformations and remain flat. At small Weber numbers, the interfacial forces balance the pressure gradient induced by the streamwise vortices even with a small deformation of the interface. In addition, for a given Reynolds number and Weber number, SHS present a larger $r_{u\phi}$ than LIS. This may be due to the larger viscosity and lower cavity Reynolds number of the lubricant in the valleys of LIS which tend to suppress fluctuations caused by the overlying streaks.

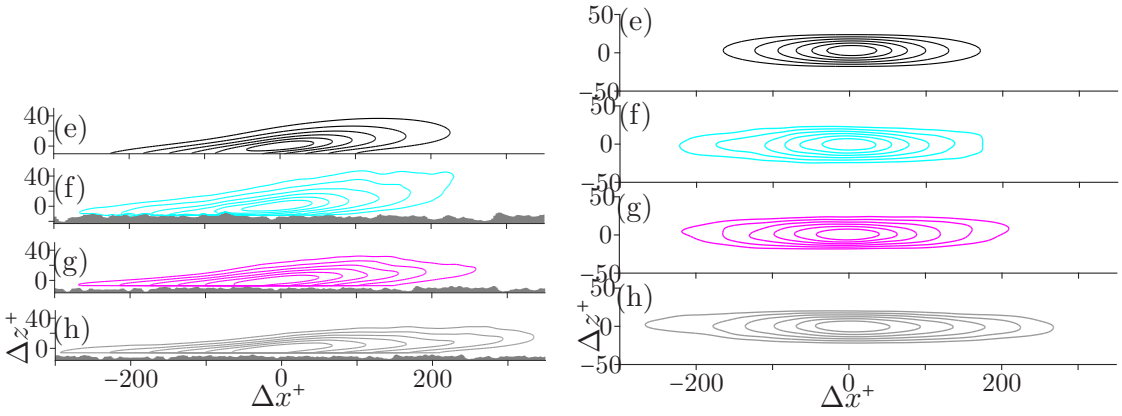

FIG. 14. Two-point streamwise velocity correlation in the x-y plane ($r_{uu}(\mathbf{x_0},\mathbf{x})$) at ($x_0 = 0.7236H, z_0 = 0.9652H$). The value of y_0 is taken 10 wall units above the interface. Contours from 0.4 to 1 with increments of 0.1: a,e) smooth wall, b,f) $k/k_{max} = 0.6$, c,g) $k/k_{max} = 0.8$, d,h) k/k_{max}=1 with $We = 0$, $Re_\tau = 395$ and $m = 0.02$ (SHS).

A quantitative analysis of the structures is performed through the two-point correlations of the streamwise velocity: $r_{uu}(\mathbf{x_0},\mathbf{x}) = \langle u(\mathbf{x_0},\mathbf{x})u(\mathbf{x})\rangle/(\tilde{u}(\mathbf{x}_0)\tilde{u}(\mathbf{x}))$, where the overbar indicates averaging with respect to time, a tilde denotes the root mean square, $\mathbf{x_0} = (x_0, y_0, z_0)$, are the coordinates of the fixed point, $\mathbf{x} = (x_0 + \Delta x, y_0 + \Delta y, z_0 + \Delta z)$ is the position of the other point. Figure 14 shows contours of r_{uu} in x, y and x, z planes respectively for

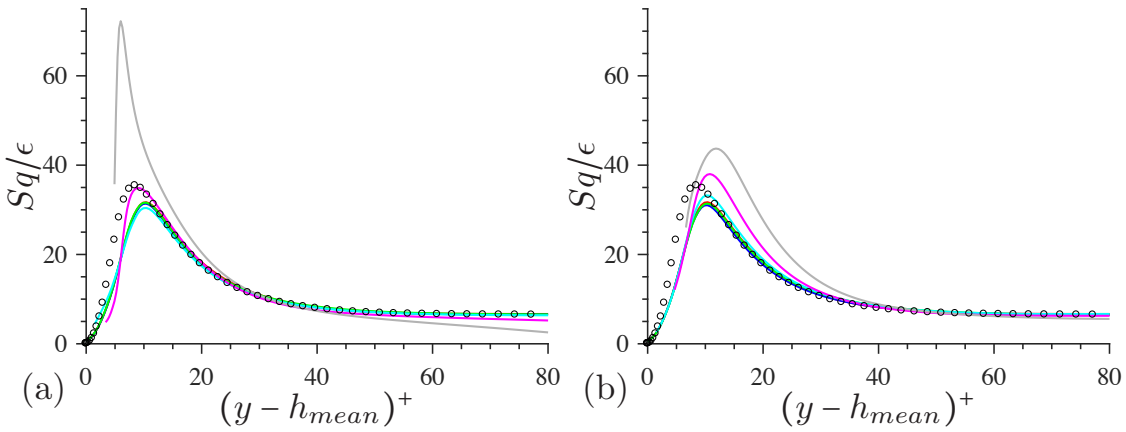

FIG. 15. Shear rate parameter (Sq/ϵ) for (a) $m = 0.02$ (SHS) and (b) $m = 0.4$ (LIS) with $Re_\tau \approx 395$ and $We = 0$ for different interface positions, (symbols and lines as in Fig. 2).

$m = 0.02$ (mimicking the viscosity ratio over SHS) and $We = 0$. Three different cases varying the position of the interface ($k/k_{max} = 0.6, 0.8, 1$) are shown and the correlation contours for the smooth wall at the same Reynolds number are shown as reference. By increasing the height of the interface, (increasing k/k_{max}), which corresponds to an increase of area fraction, volume fraction and amount of drag reduction, the structures are more elongated and less inclined with respect to the horizontal direction. The width of the structures in spanwise direction does not change much. In fact, a flat wall generates a mean velocity gradient because of the no-slip condition, which together with $\langle uv \rangle$ produces turbulent kinetic energy. In addition, it suppresses the velocity fluctuations (the velocity is zero at the wall). On the other hand, SHS and LIS tend to decrease the shear (compared to a flat wall), damp the wall normal velocity fluctuations (in the ideal case of flat slippery interface for $We = 0$, the vertical component of the velocity is zero) but not the spanwise and streamwise velocity fluctuations. Therefore, the transfer of energy from the wall-normal component of turbulence to the horizontal components typical of flat walls [34, 35] is even larger for SHS and LIS, explaining why the structures are more elongated and the increased anisotropy. This is the opposite than what has been observed for rough surfaces where the drag increases and the coherent structures are more inclined and isotropic (Leonardi *et al.* [36]).

The shear rate parameter, $S^* = Sq/\epsilon$, has been calculated to explain the increased anisotropy (where $S = d\overline{U}/dy$ is the mean shear, $q = \overline{u_i u_i}$ is twice the turbulent kinetic energy and $\epsilon = \nu\overline{(\partial u_i/\partial x_j)(\partial u_i/\partial x_j)}$ the dissipation rate of turbulent kinetic energy (Lee

et al. [37])). The shear rate parameter overlaps closely with that relative to the smooth wall in most of the channel. However, near the wall, at about $y^+ \approx 10$, for $k/k_{max} \geq 0.8$ the shear rate parameter is larger than that over the smooth wall (Fig. 15). These are in fact the cases where the streaks were more elongated and anisotropic. For example, S^* is almost twice than that over a flat surface, for $m = 0.02$ and $k/k_{max} = 1$, the case with largest drag reduction. The peak of Sq/ϵ shifts slightly towards the wall with respect to the smooth wall results. In general, consistently with the finding of Lee *et al.* [37] in homogeneous shear flows, even above SHS and LIS the streaks are strongly correlated with the shear rate parameter.

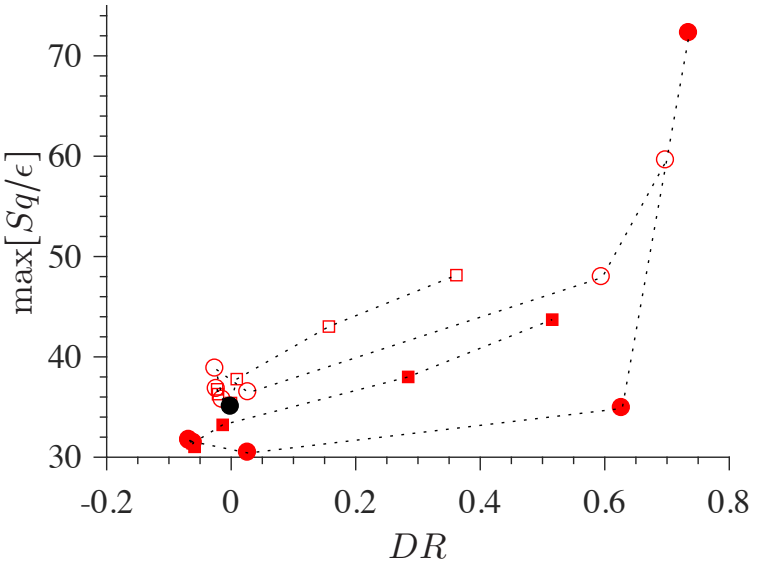

FIG. 16. Maximum of shear rate parameter Sq/ϵ as a function of drag reduction for $We = 0$: $m = 0.02$ (SHS) (○); $m = 0.4$ (LIS) (□); empty symbols $Re_\tau \approx 180$, filled symbols $Re_\tau \approx 395$, the black dot is the smooth wall.

A strong correlation between the maximum value of S^* and the amount of drag reduction is observed in Fig.16 and it is weakly dependent on the viscosity ratio and Reynolds number. To a decrease of drag ($DR > 0$) corresponds an increase of the shear rate parameter with respect to that relative to the smooth channel. The opposite occurs for drag increasing cases ($DR < 0$) when the interface is below $k/k_{max} = 0.6$.

The shear rate parameter is the ratio of the eddy turnover timescale q/ϵ and the mean shear flow timescale $1/S$. In order to explain why the shear rate parameter increases despite the drag, and the mean shear, are reduced, the value of q/ϵ and $1/S$ are compared with

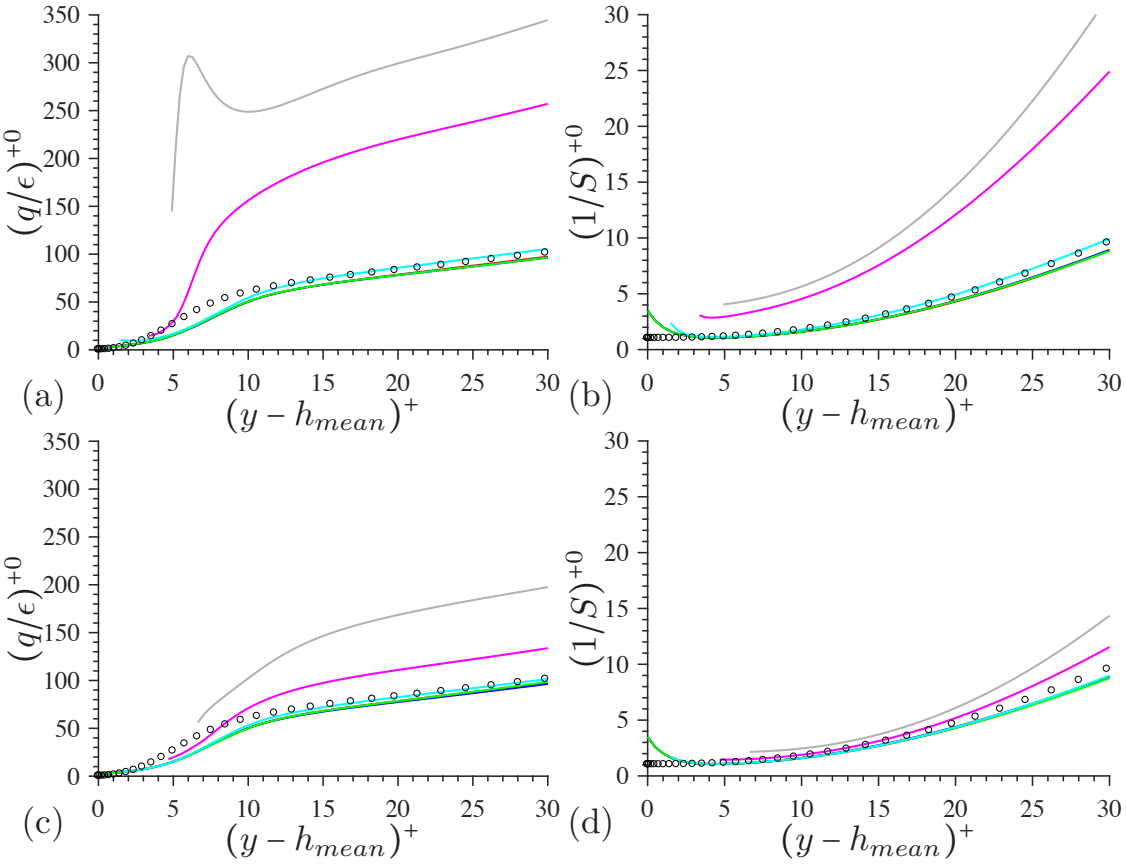

FIG. 17. (Eddy turnover timescale, (q/ϵ), (a-c) and mean shear flow time scale, $(1/S)$, (b-d) for $Re_\tau \approx 395$: (a,b) $m = 0.02$, (c,d) $m = 0.4$, (symbols and lines as in Fig. 2).

those over the smooth wall (Fig. 17). Both quantities are normalized with $H/u_{\tau 0}$ in order to have a constant factor through all the cases. When the drag reduction is approximately zero (for $k/k_{max} < 0.6$), q/ϵ and $1/S$ overlap with those relative to the smooth wall in most of the channel, with the exception of very near the interface. In correspondence of high drag reduction, on the other hand, both time scales increase significantly. However, q/ϵ increases more than $1/S$ explaining the increased shear rate parameter. The large increase of q/ϵ is due to a decrease of the dissipation of turbulent kinetic energy which overcomes that of the turbulent kinetic energy. Therefore, over drag reducing SHS and LIS, the eddy turnover time scale increases more than the mean shear flow timescale leading to an increased shear rate parameter and consequently to more elongated and anisotropic near wall structures. The peak of the eddy turnover time scale observed in Fig.17, due to the dispersive component of the turbulent kinetic energy near the wall, clarifies why the peak of Sq/ϵ shifts slightly towards the wall with respect to the smooth wall results. In fact, the dispersive component

of the turbulent kinetic energy is maximum when the slip velocity is largest as over SHS with $k/k_{max} = 1$.

VIII. CONCLUSION

Direct numerical simulations of two superposed fluids in a turbulent channel have been performed. The lower wall is made of pinnacles of random height and reproduces the etched sand blasted aluminum in Pillutla *et al.* [22]. The dynamics of the interface is fully coupled with the Navier-Stokes equations and the flow in the substrate is explicitly solved. A parametric study has been carried out varying the position of the interface, the Weber number and the Reynolds number. The detrimental contribution to the drag of the portion of the substrate emerging above the interface has been quantified. It has been found that the mean height of the texture above the interface needs to be smaller than one wall unit ($k^+_{mean} < 1$), and its root mean square, which indicates the length of the largest peaks and valleys, smaller than half wall unit ($k^+_{rms} < 0.5$). These thresholds are valid for both Reynolds numbers, viscosity ratios (SHS or LIS) and for all Weber numbers here considered. It appears that when the asperities are large, the pressure drag dominates over the Reynolds and Weber numbers. The limits $k^+_{mean} < 1$ and $k^+_{rms} < 0.5$ can be used to design SHS and LIS for practical applications. In fact, if the approximate Re_τ of the flow and the position of the interface can be estimated, k^+_{mean} and k^+_{rms} become two simple geometrical criteria for the texture. These limits can also be interpreted as a failure mechanism. When the deformation of the interface is such that the portion emerging above it is more than one wall unit, or the asperities exceed half wall unit, the drag reduction properties are lost.

Previous papers have indicated that the amount of drag reduction increases by increasing the Reynolds number. From present results, this is true only in the ideal condition of slippery and non deformable interface, i.e. in the limit of $We = 0$. In fact, when the contribution of the asperities is negligible, and the interface is slippery ($We = 0$) results are consistent with previous work, i.e. amount of drag reduction increases with Reynolds number and reduces with the viscosity ratio [1, 21, 32]. On the other hand, when the asperities emerge above the interface an increase of the Reynolds number leads to an increase of k^+_{mean} and k^+_{rms} and then to a smaller drag reduction as shown by present results. In addition, an increase of the Reynolds number leads to an increase of pressure fluctuations and therefore to a

larger deformation of the interface. This increases the drag because of a larger momentum transport inside the texture.

Present results agree well with the analytical model developed by Rastegari and Akhavan [10] between the the amount of drag reduction and slip length for all the flow conditions here considered. This is because the present texture, made of random pinnacles, induces a much weaker secondary motion than regular arrays of cubes or longitudinal bars. In addition, while for regular textures the time-averaged position of the interface is approximately flat, in this case, asperities induce local pressure gradients and a waviness of the interface. The interface is displaced downward in the regions of the substrate where the distance between the pinnacles is larger, and upward where the pinnacles are closely clustered. Oscillations with respect to this time averaged configuration are due to the passage of the streamwise vortices. In fact, a strong correlation between the instantaneous deformation of the interface and the streaks has been observed. The interface is pulled upward in proximity of low speed streaks and downward in correspondence of high speed streaks. LIS and SHS influence the near wall coherent structures similarly. The more the drag is reduced, the more the streaks become elongated and anisotropic, the larger is the shear rate parameter. When the drag is reduced both the eddy turnover timescale and the mean shear flow time scale increase. The shear rate parameter increases because the former prevails.

ACKNOWLEDGMENTS

This research was partially supported by ONR MURI grants N00014-12-01-0875 and N00014-12-01-0962. Numerical simulations were performed on TEXAS ADVANCED COMPUTING CENTER.

---

[1] Hyunwook Park, Hyungmin Park, and John Kim, "A numerical study of the effects of superhydrophobic surface on skin-friction drag in turbulent channel flow," Physics of Fluids **25** (2013).

[2] Jonathan P. Rothstein, "Slip on Superhydrophobic Surfaces," Annual Review of Fluid Mechanics **42**, 89–109 (2010).

[3] Kevin B Golovin, James W Gose, Marc Perlin, Steven L Ceccio, and Anish Tuteja, "Bioin-

spired surfaces for turbulent drag reduction," Philosophical Transactions of the Royal Society A: Mathematical, Physical and Engineering Sciences **374**, 20160189 (2016).

[4] Philseok Kim, Tak-Sing Wong, Jack Alvarenga, Michael J. Kreder, Wilmer E. Adorno-Martinez, and Joanna Aizenberg, "Liquid-Infused Nanostructured Surfaces with Extreme Anti-Ice and Anti-Frost Performance," ACS Nano **6**, 6569–6577 (2012).

[5] Elias Aljallis, Mohammad Amin Sarshar, Raju Datla, Vinod Sikka, Andrew Jones, and Chang Hwan Choi, "Experimental study of skin friction drag reduction on superhydrophobic flat plates in high Reynolds number boundary layer flow," Physics of Fluids **25** (2013).

[6] Rahul A. Bidkar, Luc Leblanc, Ambarish J. Kulkarni, Vaibhav Bahadur, Steven L. Ceccio, and Marc Perlin, "Skin-friction drag reduction in the turbulent regime using random-textured hydrophobic surfaces," Physics of Fluids **26** (2014).

[7] Hangjian Ling, Siddarth Srinivasan, Kevin Golovin, Gareth H. McKinley, Anish Tuteja, and Joseph Katz, "High-resolution velocity measurement in the inner part of turbulent boundary layers over super-hydrophobic surfaces," Journal of Fluid Mechanics **801**, 670–703 (2016).

[8] Siddarth Srinivasan, Justin A. Kleingartner, Jonathan B. Gilbert, Robert E. Cohen, Andrew J.B. Milne, and Gareth H. McKinley, "Sustainable Drag Reduction in Turbulent Taylor-Couette Flows by Depositing Sprayable Superhydrophobic Surfaces," Physical Review Letters **114**, 014501 (2015).

[9] Jongmin Seo and Ali Mani, "Effect of texture randomization on the slip and interfacial robustness in turbulent flows over superhydrophobic surfaces," Physical Review Fluids **3**, 044601 (2018).

[10] Amirreza Rastegari and Rayhaneh Akhavan, "On the mechanism of turbulent drag reduction with super-hydrophobic surfaces," Journal of Fluid Mechanics **773**, R4 (2015).

[11] J. Seo, R. García-Mayoral, and A. Mani, "Pressure fluctuations and interfacial robustness in turbulent flows over superhydrophobic surfaces," Journal of Fluid Mechanics **783**, 448–473 (2015).

[12] J. Seo, R. García-Mayoral, and A. Mani, "Turbulent flows over superhydrophobic surfaces: flow-induced capillary waves, and robustness of airwater interfaces," Journal of Fluid Mechanics **835**, 45–85 (2018).

[13] E.J. García-Cartagena, I. Arenas, M. Bernardini, and S. Leonardi, "Dependence of the drag over super hydrophobic and liquid infused surfaces on the textured surface and weber number,"

Flow, Turbulence and Combustion **100**, 945–960 (2018).

[14] Jeong Hyun Kim and Jonathan P. Rothstein, "Delayed lubricant depletion on liquid-infused randomly rough surfaces," Experiments in Fluids **57**, 81 (2016).

[15] Karim Alamé and Krishnan Mahesh, "Wall-bounded flow over a realistically rough superhydrophobic surface ," J. Fluid Mech. **873**, 977–1019 (2019).

[16] Mark Sussman, Peter Smereka, and Stanley Osher, "A Level Set Approach for Computing Solutions to Incompressible Two-Phase Flow," Journal of Computational Physics **114**, 146–159 (1994).

[17] P. Orlandi, *Fluid Flow Phenomena: A Numerical Toolkit*, Vol. 55 (Springer, 2000).

[18] J. A. Sethian and P. Smereka, "Level set methods for fluid interfaces," Annual Review of Fluid Mechanics **35**, 341–372 (2003).

[19] G. Russo and P. Smereka, "A remark on computing distance functions," Journal of Computational Physics **163**, 51–67 (2000).

[20] Yuriko Renardy and Michael Renardy, "PROST: A Parabolic Reconstruction of Surface Tension for the Volume-of-Fluid Method," Journal of Computational Physics **183**, 400–421 (2002).

[21] Isnardo Arenas, Edgardo García, Matthew K. Fu, Paolo Orlandi, Marcus Hultmark, and Stefano Leonardi, "Comparison between super-hydrophobic, liquid infused and rough surfaces: a direct numerical simulation study," Journal of Fluid Mechanics **869**, 500–525 (2019).

[22] V. Pillutla, H. Ling, L. Rodriguez, D.B.C. Rodriguez, J. Katz, and W. Choi, "Robust Drag Reduction Superhydrophobic Surfaces with Large Slip Lengths," 31st Symposium on Naval Hydrodynamics (2016).

[23] P. Orlandi and S. Leonardi, "DNS of turbulent channel flows with two- and three-dimensional roughness," Journal of Turbulence **7**, N73 (2006).

[24] M. Thakkar, A. Busse, and N. D. Sandham, "Direct numerical simulation of turbulent channel flow over a surrogate for Nikuradse-type roughness," Journal of Fluid Mechanics **837**, R11–R111 (2018).

[25] R. D. Moser, J. Kim, and N.N. Mansour, "Direct numerical simulation of turbulent channel flow up to $Re_\tau = 590$," Physics of Fluids **11**, 943–945 (1999).

[26] Hangjian Ling, Siddarth Srinivasan, Kevin Golovin, Venkata Pillutla, Gareth H Mckinley, Anish Tuteja, Wonjae Choi, and Joseph Katz, "Flow Structure and Turbulence in the Inner Part of Turbulent Boundary Layers over Super-Hydrophobic Surfaces," 31st Symposium on

Naval Hydrodynamics (2016).

[27] A. E. Perry and P.N. Joubert, "Rough wall boundary layers in adverse pressure gradients." J. Fluid Mech. **17**, 193–211 (1963).

[28] S. Leonardi, P. Orlandi, R. J. Smalley, L. Djenidi, and R. a. Antonia, "Direct numerical simulations of turbulent channel flow with transverse square bars on one wall," Journal of Fluid Mechanics **491**, 229–238 (2003).

[29] P. S. Jackson, "On the displacement height in the logarithmic velocity profile," Journal of Fluid Mechanics **111**, 15–25 (1981).

[30] Eric Lauga and Howard A. Stone, "Effective slip in pressure-driven Stokes flow," Journal of Fluid Mechanics **489**, 55–77 (2003).

[31] Paolo Luchini, Fernando Manzo, and Amilcare Pozzi, "Resistance of a grooved surface to parallel flow and cross-flow," Journal of Fluid Mechanics **228**, 87–109 (1991).

[32] M K Fu, I Arenas, S Leonardi, and M Hultmark, "Liquid-infused surfaces as a passive method of turbulent drag reduction," Journal of Fluid Mechanics **824**, 688–700 (2017).

[33] Amirreza Rastegari and Rayhaneh Akhavan, "On drag reduction scaling and sustainability bounds of superhydrophobic surfaces in high Reynolds number turbulent flows," Journal of Fluid Mechanics **864**, 327–347 (2019).

[34] JCR Hunt and JMR Graham, "Free-stream turbulence near plane boundaries," Journal of Fluid Mechanics **84**, 209–235 (1978).

[35] Moon Joo Lee and J. C. R. Hunt, "The structure of sheared turbulence near a plane boundary," in *Turbulent Shear Flows 7*, edited by Franz Durst, Brian E. Launder, William C. Reynolds, Frank W. Schmidt, and James H. Whitelaw (Springer Berlin Heidelberg, 1991) pp. 101–118.

[36] Stefano Leonardi, Paolo Orlandi, Lyazid Djenidi, and Robert A. Antonia, "Structure of turbulent channel flow with square bars on one wall," International Journal of Heat and Fluid Flow **25**, 384–392 (2004).

[37] Moon Joo Lee, John Kim, and Parviz Moin, "Structure of turbulence at high shear rate," Journal of Fluid Mechanics **216**, 561 (1990).